Effect of Reactant-Surface Stretching on Chemical Laser Performance

Richard J. Driscoll*
Bell Aerospace Textron, Buffalo, New York

High-pressure DF chemical lasers use gas trip jets to increase the laser cavity reactant mixing rate. The trip jets can improve the laser efficiency by about 100% when compared to the laminar mixing value. It is postulated that the trip jets create a secondary flow which increases the mixing rate by stretching the contact surface between the reactant streams. The surface stretching rate can be described in terms of a strain rate s_0. A qualitative explanation for the performance characteristics of trip-nozzle lasers is provided herein by developing flow and laser models which can define the effect of strain on the reactant burning rate and laser efficiency. Strain affects laser performance via a single parameter $\gamma = 2s_0/k_c$, where k_c is a characteristic collisional deactivation rate for the lasing specie. Strain levels of $\gamma = 2$-3 appear to be consistent with trip nozzle data. The model also indicates the efficiency of low-pressure laminar mixing ($\gamma = 0$) lasers could be increased significantly for strain rate levels in the $\gamma = 3$-5 range.

Nomenclature

B_1,B_2,B_3 = constants, $B_1 = (\rho_2/\rho_1)B_2$; B_3 defined by Eq. (19)
C_1,C_2,C_3 = constants in gain equation, see Eq. (10)
D_1,D_2,D_3 = constants, $D_1 = K_1/K_3$, $D_2 = K_2/K_3$
D = molecular diffusivity
f_1,f_2 = functions in amplifier solution, Eq. (22)
F = $(y_f/w)^2$, normalized flame location
g,g_0 = gain per unit length, $g_0 = \sigma[F]_1$
G = integrated gain across flow channel, Eq. (16)
G^* = $G/(g_0 w)$, normalized integrated gain
G_t^* = $-\ln(r_1 r_2)/(4Ng_0 w)$, threshold gain
I = radiation intensity
k_c^*,k_p^* = kinetic rates for collisional deactivation and pumping, cm^3/mole-s
k_c,k_p = $[\ ]\ k_i^*$, kinetic rate concentration product, s^{-1}
K_1 = k_p/k_c, (pumping/deactivation) rate ratio
K_2 = $2\sigma/(\epsilon k_c)$, (stimulated emission/deactivation) rate ratio
K_3 = $1 + K_2$
L,L_0 = fluid element length scale, see Fig. 2
M_i = ith specie molecular weight
N_A = Avagadro's number
p = pressure
P = laser power, Eq. (17)
P^* = $\zeta_d^{1/2}\eta$, normalized power per channel
r = y_f^*/w, volume fraction of oxidizer burned
r_1,r_2 = mirror reflectivities
$s(x)$ = $\partial w/\partial z$, axially varying linear strain rate
s_0 = characteristic constant linear strain rate
t = x/u, flow time
t_b = strained flow oxidizer element burnout time
t_d = $0.25\,(w/B_1)^2/D$, laminar burnout time
T = temperature
u = constant axial flow velocity
V = (u,v,w), velocities for coordinates fixed in fluid element, see Fig. 2
$w_1(x),w_2(x)$ = oxidizer and fuel element widths
w = $w_1(0)$, initial oxidizer element width
x = (x,y,z), coordinates fixed in element, see Fig. 2
x^* = (x^*,y^*,z^*), coordinates fixed in nozzle, see Fig. 1
x_b,x_d = ut_b, ut_d, characteristic distances
X_i = ith specie mole fraction
y_f = flame location, Eq. (9) and Fig. 2
y_f^* = $wr(x)$, effective flame location for strained flow
Y_i, Y_i^o = ith specie mass fraction, initial values
γ = $2s_0/k_c$, (strain/deactivation) rate ratio
ϵ = $h\nu N_A$, energy per mole of photons
ζ = xk_c/u, normalized axial distance
ζ_b,ζ_d = $x_b k_c/u$, $x_d k_c/u$, characteristic distances
ζ_i,ζ_e = start and end of lasing region in oscillator solution
ζ_0 = axial location of flame with penetration y_f
ζ_{dj} = value of ζ_d for which $r_e(\zeta_d) = 1$, i.e., when $\zeta_d = \zeta_{dj}$, $\zeta_e = \zeta_b$
η = transverse coordinate, see Eq. (3), or normalized laser efficiency (η_c/η_0), see Eq. (18)
η_0 = efficiency for a premixed saturated laser
η_c = $\eta\eta_0$, chemical efficiency
λ = $2s_0 t_d = \zeta_d\gamma$, strain-laminar mixing time product
ξ,ξ_0 = $\eta + B_2, B_2$, transverse coordinate
ρ = density
σ = stimulated emission cross section
τ = t/t_d, normalized time
τ_b = t_b/t_d, normalized burnout time
φ_i = $\zeta_d^{1/2} G_t^*$, threshold gain parameter
$[\ ]$ = concentration, mole/cm^3

Subscripts

1,2 = oxidizer stream, fuel stream, see Fig. 2
b = location where all oxidizer is consumed
d = laminar mixing value
e = end of lasing region for oscillator
f = property at flame
i = start of lasing region for oscillator
r = reference value

Received May 13, 1982; revision received Oct. 25, 1982.

*Group Leader, Laser Fluid Mechanics. Member AIAA.

I. Introduction

GENERALLY, cw DF chemical lasers operate in the mixing-limited regime. Available analyses[1,2] indicate that a high laser efficiency requires a reactant mixing rate

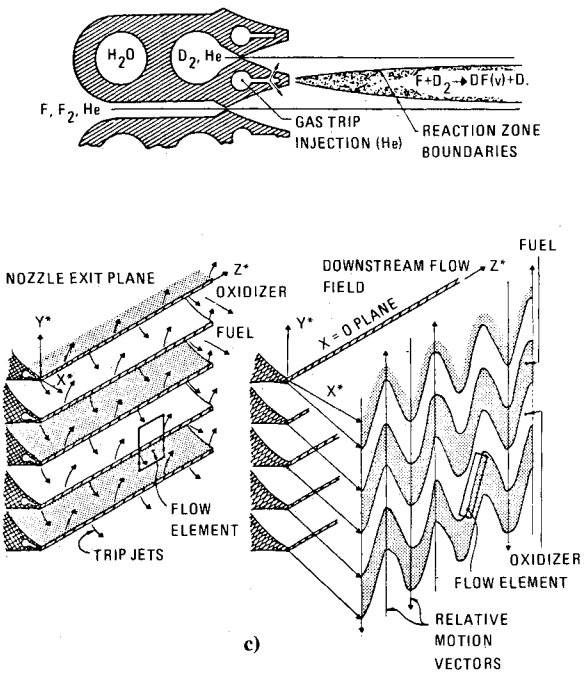

Fig. 1 Trip nozzle geometry and flowfield model: a) nozzle geometry; b) trip jet configuration; and c) downstream flowfield.

which is fast compared to the lasing specie collisional deactivation rate. At very low cavity pressures, $p \ll 133$ N/m^2 (1 Torr), diffusional mixing is fast compared to deactivation and the laser efficiency approaches that of a premixed laser. At very low pressures, laser power densities are too low for practical high-power laser systems and, thus, low-pressure lasers are usually operated in the $133 \leq p \leq 665$ N/m^2 ($1 \leq p \leq 5$ Torr) cavity pressure range where the joint requirements on laser efficiency and power density can be satisfied. In this regime, the laminar mixing and collisional deactivation rates are of the same order. Laser efficiencies are high but well below premixed limits. In this paper, we will indicate how the efficiencies for this type of laser can be increased.

When a high-pressure recovery level is a laser system requirement, then the laser must be operated at a high-cavity pressure, $p > 1333$ N/m^2 (10 Torr). In this regime, laminar mixing is relatively slow and the mixing rate must be increased above the laminar value if the laser is to operate efficiently. The so-called trip nozzle, shown in Fig. 1, has been developed for this purpose. In this nozzle design, gas injection at the nozzle exit plane is used to perturb the reactant streams and accelerate the mixing rate. The use of the trip jet concept on a chemical laser was first demonstrated by Witte et al.[3] Wilson and Hook[4] report that trip jet injection produced an 80% increase in laser power when compared to the laminar mixing case while Driscoll and Tregay[5] present photographic data showing the trip jets reduce the reactant mixing lengths from about 5 cm for laminar mixing to about 1 cm with trip jet injection. Thus, available data shows clearly that the trip jets increase mixing and performance for high-pressure lasers; what is not apparent, however, is the mechanism by which they do this.

It could be supposed that the gas jets accelerate the laminar-to-turbulence transition which occurs naturally in these shear layers and, indeed, this is the reason these gas jets are commonly called trip jets. The measurement of Cenkner[6] indicates, however, that the turbulence levels in the laser cavity are not significantly increased by the gas jets. Thus, the use of turbulent mixing arguments to explain the trip jet mixing mechanism has no foundation. Clearly, the name trip jet is a misnomer; however, we shall continue to use it since it is the term commonly used within the chemical laser community.

To date, a plausible mechanistic model for trip jet mixing has not been reported; current flow models are heuristic in nature. The most common approach[5,7] to describing the trip mixing rate is simply to increase the molecular diffusion coefficient to a level which yields agreement with laser power and gain data. Herein, we develop a mechanism based on the idea that the trip jets produce a secondary transverse flow in the laser cavity which stretches the contact surfaces between the reactant streams. This contact area increase, to which the mixing rate is proportional, can be described in terms of an induced linear strain rate. In Sec. II, we develop a flame model for burning in the presence of a linear strain field and use this model in Sec. III to develop a laser performance model which can describe qualitatively the influence of strain rate on the laser efficiency. It is shown in Sec. IV that the strained flow laser model is in qualitative agreement with trip nozzle data and that the performance of low-pressure laminar mixing nozzle designs could be increased significantly if strain could be generated in their flowfield.

II. Flow Model

Trip Flow Model

Figure 1 shows the trip nozzle flowfield. Alternating supersonic streams containing fuel, oxidizer, and diluent enter the laser cavity and start to react at $x^* = 0$. For the DF laser depicted in Fig. 1a, the laser fuel is deuterium (D_2), the oxidizer is atomic fluorine (F), and the diluent is helium. The laser pumping reaction $D_2 + F \rightarrow DF(v) + D$, $v = 1\text{-}4$, creates vibrationally excited DF which can be made to lase in a suitable optical cavity.

Figure 1b shows a sketch of the nozzle with the arrows indicating the location and injection direction of the trip jets. The trip jets are located along the edges of the nozzle blades and alternate in their direction of injection. Let $x^* = (x^*, y^*, z^*)$ be the coordinate system fixed on the nozzle. The trip jets in any (x^*, y^*) plane all point in the same direction with the injection direction alternating between $(+y^*)$ and $(-y^*)$ as one moves along the blade in the z^* direction. At their injection point, the trip jets are highly underexpanded to ensure that the jets penetrate well into the nozzle flow. Consider a jet whose injection direction is $(+y^*)$ into the oxidizer nozzle stream. The data of Zukoski and Spaid[8] show that the static pressure on the windward side of the jet is much higher than that in the freestream, while the pressure on the lee side of the jet is significantly lower than the freestream pressure. Thus, the trip jet tends to push oxidizer material in the $(+y^*)$ direction while the low pressure on the lee side tends to induce a cross flow of material from the fuel stream also in the $(+y^*)$ direction. The net effect is to give the fuel and oxidizer material in the neighborhood of the jet a $(+y^*)$ velocity component. Since the trip jets in neighboring (x^*, y^*) planes alternate in their orientation, the transverse velocity induced by the trip jets will alternate from the $(+y^*)$ to $(-y^*)$ direction as one moves along the blade. The effect of this secondary motion is to stretch the material from the fuel and oxidizer nozzles into the elongated and rippled shape shown in Fig. 1c. If the flow pictured in Fig. 1c were photographed from outside the laser cavity with the camera axis parallel to the z^* direction, one would see well-defined reaction zone boundaries moving from the nozzle lips toward the centerlines of both nozzles as a result of the transverse convection. Reacting material on the nozzle centerlines at any x^* location does not now imply complete mixing at that location. Thus, the model of Fig. 1c provides a possible explanation for the short mixing length data of Driscoll and Tregay.[5]

A flow element bounded by two trip jets and the nozzle centerlines is shown in Figs. 1b and 1c. The effect of the transverse convection is to rotate and stretch the element. The element stretching increases the reaction rate by increasing the contact area between the reactant streams and also by reducing the transverse mixing scales below the levels imposed

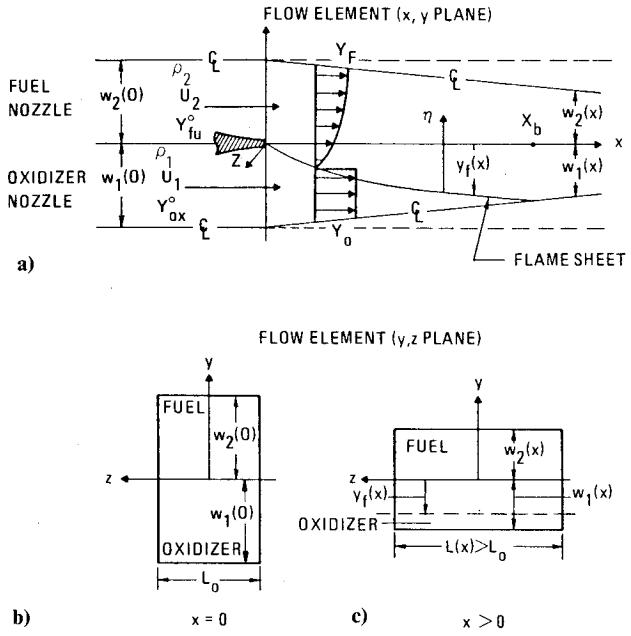

Fig. 2 "One boundary-layer" strained flow model: a) flow model; b) element at $X=0$; and c) stretched element at $X>0$.

by the nozzle geometry. The rate at which the element is stretched can be described in terms of the strain rate induced by the trip jets and we turn now to that problem.

Problem Formulation

We consider the flow element shown in Figs. 1b and 1c and inquire as to how the reactants in this element burn in the presence of a strain field. Chemical laser flows are usually fuel rich and the flame which forms at $x^*=0$ moves into the oxidizer-bearing material. To solve this problem, we use the model shown in Fig. 2 where the coordinates $x=(x,y,z)$ are fixed in the fluid element; note $x^*=x$. The principal strain axis along which the element is stretched is z while element compression occurs along the y axis. Figure 2a shows the (x,y) plane through the element with the flame $y_f(x)$ moving into the oxidizer stream. The element boundaries $w_1(x)$ and $w_2(x)$ move toward the centerline due to the strain-induced convection. Figures 2b and 2c show the (y,z) planes of the element at $x=0$ and $x>0$, respectively, and indicate how the strain field distorts the element and increases the contact area between the fuel and oxidizer. All the oxidizer is reacted when $y_f(x_b)=w_1(x_b)$, x_b being the axial distance for oxidizer burnout.

The mass conservation equation for the fluid element is $\nabla(\rho V)=0$. $V=(u,v,w)$ is the velocity with respect to the local coordinate system x. We assume the axial velocities from the fuel and oxidizer nozzles are uniform (the boundary layers are neglected), identical, and invariant with axial distance, i.e., $u_1=u_2=u=\text{const}$. This presumes negligible heat release within the laser cavity or a constant pressure flow. From the flow geometry shown in Fig. 1, the gradients of the scalar variables in the z direction will be small compared to those in the y direction; thus, the gas density will satisfy $\rho=\rho(x,y)$, $\rho\neq\rho(z)$. With these constraints, the continuity equation can be written as

$$\frac{\partial(\rho v)}{\partial y}=-u\frac{\partial\rho}{\partial x}-\rho s(x) \tag{1}$$

where $s(x)$ represents the induced strain rate $s=\partial w/\partial z$ which can vary in the axial direction.

Within the context of boundary-layer theory, the transport equation for the ith specie mass fraction Y_i is

$$\rho u\frac{\partial Y_i}{\partial x}+\rho v\frac{\partial Y_i}{\partial y}=\frac{\partial}{\partial y}\left(\rho D\frac{\partial Y_i}{\partial y}\right)+\omega_i \tag{2}$$

where ω_i is the chemical source term and D is the molecular diffusivity (taken equal for all species). We further assume that $\rho^2D=\rho_r^2D_r$ where subscript r indicates a reference value; this approximation is satisfied reasonably well in constant pressure gas flows. We now invoke the flame sheet approximation wherein it is assumed that the kinetic time scale for the laser pumping reaction is small compared to the flow time. The pumping reaction then goes to completion in the neighborhood of a thin flame and $\omega_i=0$ except in this region. Thus, we solve Eq. (2) for the regions $y<y_f$ and $y>y_f$ with $\omega_i=0$; the influence of the flame on the solution for Y_i is defined using the flame sheet boundary conditions. The solution is obtained in terms of the similarity coordinate

$$\eta=\frac{B_1}{y_f}\int_{y_f}^{y}\frac{\rho}{\rho_2}\,dy \tag{3}$$

where $y_f(x)$ defines the flame location and B_1 is a constant. Using the results just given and $\rho_r=\rho_2$, then Eq. (2) can be written as

$$u\frac{\partial Y_i}{\partial x}+\left[u\frac{\partial\eta}{\partial x}+B_1\frac{\rho v}{\rho_2 y_f}\right]\frac{\partial Y_i}{\partial\eta}=\left(\frac{B_1}{y_f}\right)^2D_r\frac{\partial^2Y_i}{\partial\eta^2} \tag{4}$$

The continuity equation can be integrated from y_f to y to obtain an expression for the bracketed term in Eq. (4). Thus, Eq. (4) becomes

$$u\frac{\partial Y_i}{\partial x}+B_1\left[\frac{\rho_f}{\rho_2}\left(\frac{v_f}{y_f}-\frac{u}{y_f}\frac{dy_f}{dx}\right)\right.$$

$$\left.-\frac{\eta}{B_1}\left(s+\frac{u}{y_f}\frac{dy_f}{dx}\right)\right]\frac{\partial Y_i}{\partial\eta}=\left(\frac{B_1}{y_f}\right)^2D_r\frac{\partial^2Y_i}{\partial\eta^2} \tag{5}$$

where v_f is the transverse velocity at the flame. Further progress in solving Eq. (5) requires definition of the flame sheet boundary conditions.

One Boundary-Layer Flame Sheet Model

To simplify the solution of Eq. (5), we will adopt the "one boundary-layer" approximation introduced by Hofland and Mirels.[9] In this model, it is assumed that the fluorine diffuses to the flame at a rate which is slow compared to the fuel diffusion rate, this being due to the approximate factor of two difference in the diffusion coefficients for the two species. Thus, on the oxidizer side of the flame ($\eta<0$), conditions are uniform at their nozzle exit values. A diffusion layer forms on the fuel side ($\eta>0$); we need solve Eq. (5) only for this region. It is now appropriate to set $D_r=D$ where D is the diffusion coefficient for the fuel in stream 2.

On the oxidizer side of the flame sheet, the transverse velocity and density are $v=-sy_f$ and ρ_1, respectively, while the values on the fuel side of the flame are v_f and ρ_f. The continuity equation indicates the quantity $\rho(udy/dx-v)$ is constant across the flame; thus, $(\rho v)_f$ can be written as

$$\frac{(\rho v)_f}{\rho_1}=\left(\frac{\rho_f}{\rho_1}-1\right)u\frac{dy_f}{dx}-sy_f \tag{6}$$

Using Eq. (6) in Eq. (5) yields

$$\frac{\partial^2 Y_i}{\partial \eta^2} + \left(\eta + B_1 \frac{\rho_1}{\rho_2}\right)\left[\frac{y_f^2}{B_1^2 D}\left(s + \frac{u}{y_f}\frac{dy_f}{dx}\right)\right]\frac{\partial Y_i}{\partial \eta} = \frac{u y_f^2}{B_1^2 D}\frac{\partial Y_i}{\partial x} \quad (7)$$

Equation (7) has a similarity solution of the form $Y_i = Y_i(\eta)$ if the bracketed term in Eq. (7) can be taken as constant; note, since $y_f = y_f(x)$ and $s = s(x)$, the bracketed term cannot be a function of η. Since B_1 is an as yet undefined constant, we can set the bracketed term to any arbitrary nonzero value without affecting the solution; for convenience, we choose 2. Defining $B_2 = B_1\rho_1/\rho_2$, $\xi = \eta + B_2$, and $\xi_0 = B_2$, then Eq. (7) reduces to

$$\frac{d^2 Y_i}{d\xi^2} + 2\xi\frac{dY_i}{d\xi} = 0 \quad (8)$$

and y_f is now given by

$$\frac{dy_f^2}{dx} + 2\frac{s y_f^2}{u} = 4B_1^2\left(\frac{D}{u}\right) \quad (9)$$

Note that the strain rate $s(x)$ appears only in Eq. (9). The constants B_1 and B_2 are functions of the reactant stoichiometry and are obtained by solving Eq. (8). The quantity (B_1/y_f) needed to calculate η from Eq. (3) can be obtained from Eq. (9); note, (B_1/y_f) is independent of the reactant stoichiometry but does depend on the strain rate distribution $s(x)$.

Consider the fuel mass fraction Y_{fu}. At the flame, $Y_{fu} = 0$ since by definition neither fuel nor oxidizer exist at the flame. At the nozzle exit plane $Y_{fu} = Y_{fu}^o$. To conform with the solutions of Hofland and Mirels,[9] we use the boundary conditions $\eta = 0$, $\xi = \xi_0$, $Y_{fu} = 0$ and $\eta \to \infty$, $\xi \to \infty$, $Y_{fu} = Y_{fu}^o$; this presumes a fuel-rich flow and $w_2 \gg w_1$. It easily is shown that the solution for Y_{fu} is $Y_{fu}/Y_{fu}^o = [\mathrm{erf}(\xi) - \mathrm{erf}(\xi_0)]/\mathrm{erfc}(\xi_0)$, where erf( ) is the error function and erfc( ) = 1 − erf( ).

At the flame, fuel diffusion balances oxidizer convection and stoichiometry dictates that

$$\frac{d}{d\xi}\left(\frac{Y_{fu}}{Y_{fu}^o}\right)_f = -\frac{2B_2}{B_3}, \qquad B_3 = \frac{\nu_{ox} M_{ox} Y_{fu}^o}{\nu_{fu} M_{fu} Y_{ox}^o} \quad (10)$$

where ν_i are the stoichiometric coefficients for the reaction, $\nu_{fu}(\text{fuel}) + \nu_{ox}(\text{oxidizer}) \to \nu_p(\text{product})$ and M_i are the specie molecular weights. Using the solution for $Y_{fu}(\xi)$, it is easily shown that Eq. (10) yields $B_2\exp(B_2^2)\mathrm{erfc}(B_2) = -B_3/\pi^{1/2}$; clearly, $B_2 < 0$ and, thus, $\xi_0 < 0$. Hofland and Mirels[9] obtain this same result in their study of laminar flames and they indicate that, for $10 \le \xi_0 \le 10^3$, ξ_0 can be approximated by $-\xi_0 = 0.45 + 0.60\log_{10}(B_3)$.

For laminar mixing, $s = 0$ and Eq. (9) yields

$$y_f(x) = 2B_1\left(\frac{Dx}{u}\right)^{1/2} = 2B_2\left(\frac{\rho_2}{\rho_1}\right)\left(\frac{Dx}{u}\right)^{1/2} \quad (11)$$

When $s = 0$, then $w_1(x) = w_1(0) = \text{const}$. Since the fuel nozzle size is no longer a parameter in the problem, we define $w = w_1(0)$ as the characteristic nozzle scale. Solving Eq. (11) for the burnout location x_d and time t_d (subscript d indicates laminar mixing results and b the strained flame case) yields $x_d = ut_d = 0.25(u/D)(w/B_1)^2$.

Flame Location with Strain

With $t = x/u$, $\tau = t/t_d$, and $F = (y_f/w)^2$, then Eq. (9) can be written as $dF/d\tau + 2st_dF = 1$. If $(st_d) \ll 1$, then the influence of strain on y_f is negligible and the solution reduces to Eq. (11). Defining a strain rate parameter $\lambda = 2st_d$, and using the initial condition $F(0) = 0$, then the solution for $F(\tau)$ is

$$F = \exp(-\beta)\int_0^\tau \exp(\beta)\,d\tau, \qquad \beta(\tau) = \int \lambda(\tau)\,d\tau \quad (12)$$

Note that when $s(\tau) = \text{const}$, then $F(\tau)$ has a steady-state solution which implies at $t \to \infty$, $(y_f/w) \to 1/\lambda^{1/2}$; for this case, strain balances diffusion and the flame becomes stationary.

Since $v = -sy$ on the oxidizer side of the flame, then the motion of the symmetry line $w_1(x)$ is described by $dw_1/dt = -sw_1$. With $w_1(0) = w$, it easily is shown that $w_1(\tau)/w = \exp(-\beta/2)$. From the definition of $s(x)$, it easily is shown that the lateral extension of the element is $L(\tau)/L_0 = \exp(\beta/2)$. Thus, the area of the oxidizer side of the element is constant, i.e., $L(\tau)w_1(\tau) = L_0 w$.

For the remainder of this analysis, we assume the strain rate is constant, i.e., $s(x) = s_0$. Thus, $\lambda = 2s_0t_d$, $\beta = \lambda\tau$, $w_1/w = \exp(\lambda\tau/2)$, and $y_f/w = [1 - \exp(-\lambda\tau)]^{1/2}/\lambda^{1/2}$. The oxidizer is completely burned when $y_f(x_b) = w_1(x_b)$. Defining a nondimensional burnout time by $\tau_b = t_b/t_d$, then it easily is shown that $\tau_b = \lambda^{-1}\ell_n(1+\lambda)$. As $\lambda \to 0$, $\tau \to 1$, i.e., the laminar result is recovered. For $\lambda = 10$, $\tau_b = 0.24$; this indicates the potential for strain to reduce the burn time. The element compression and extension at burnout are given by $L(\tau_b)/L_0 = (1+\lambda)^{1/2}$ and $w_1(\tau_b)/w = (1+\lambda)^{-1/2}$; for $\lambda = 10$, $L/L_0 = 3.32$, i.e., the contact area between the reactant streams has increased by more than a factor of three at burnout.

For the laser analysis which follows, it is necessary to describe the volume fraction of the oxidizer stream which has been burned; the ratio (y_f/w) does this only for the laminar flame case. Let $r(\tau)$ be the fraction of the oxidizer which has been burned and let $y_f^*(\tau)$ be the effective flame location defined such that $r(\tau) = y_f^*(\tau)/w$. From Fig. 2c, we have $r(\tau) = y_f(\tau)L(\tau)/(L_0 w)$ which for the constant strain model implies $r(\tau) = [\exp(\lambda\tau) - 1]^{1/2}/\lambda^{1/2}$. As $\lambda \to 0$, $r(\tau) \to \tau^{1/2}$ and the laminar results are recovered. Note, also, that when $(\lambda\tau) \ll 1$, the burning rate is effectively laminar. Figure 3 shows $r(\tau)$ for $0 \le \lambda \le 25$ and provides an indication as to the effectiveness of flame stretch in reducing the burn time.

III. Laser Model

The two-level laser model of Mirels et al.[1] forms the starting point for our analysis. Mirels et al.[1] calculate laser performance for flame shapes of the class $y_f \sim x^n$. The flame model developed in Sec. II does not fit within this class. We, therefore, generalize the results given in Ref. 1 for arbitrarily shaped flames and then use the results given in Sec. II to define the influence of strain on laser performance. Both

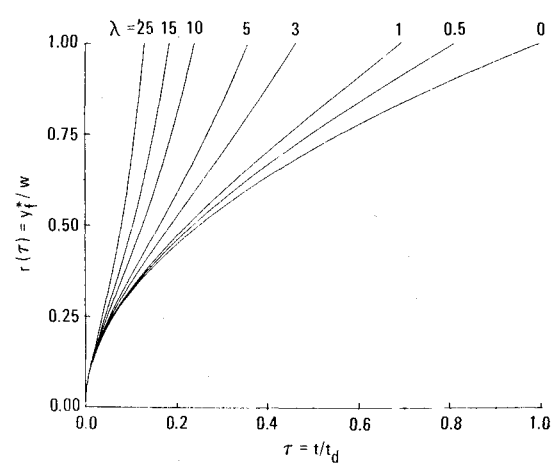

Fig. 3 Flame function vs time, $0 \le \lambda \le 25$.

Broadwell[2] and Mirels[10] have developed models which treat the multiple vibrational level lasing which occurs in HF and DF lasers; in addition, the model of Mirels[10] is developed for flames of arbitrary shape although he presents results only for the $y_f \sim x^n$ class. These more complex models are not required to illustrate the effect of strain on laser performance. We, therefore, use the simple two-level model since it is adequate for the purposes of this analysis. Mirels[10] indicates that the results from the multivibrational level models can be recovered from the two-level model by simply redefining model parameters and the reader is referred to that paper for details. Space limitations preclude detailed derivations herein; we, therefore, refer the reader to Refs. 1, 2, 10, and 11 for background material.

In the two-level DF laser model, the local media gain is $g=\sigma([DF_u]-[DF_l])$ where σ is the stimulated emission cross section and $[DF_u]$ and $[DF_l]$ are the upper and lower laser level molar concentrations. If all the fluorine is burned at the flame, then just downstream of the flame $[DF_u]=[F]_I$ where $[F]_I$ is the fluorine atom concentration in the oxidizer stream. We define a characteristic gain $g_0=\sigma[F]_I$; g_0 is the gain just downstream of the flame in the limit of $k_p^* \to \infty$ where k_p^* is the forward kinetic rate for the reaction $F+D_2 \to DF_u+D$. Since the flow is fuel rich, we define the effective pumping rate by $k_p=k_p^*[D_2]_2$ where $[D_2]_2$ is the deuterium concentration in the fuel stream. Molecules are removed from the upper state via the collisional deactivation step $DF_u+M \to DF_l+M$ where M is a collisional partner; if k_c^* is the kinetic rate for this step, then a characteristic deactivation rate can be defined by $k_c=k_c^*[M]$. Note, k_p and k_c have units of time^{-1}. The parameter $K_1=k_p/k_c$ represents the pumping to deactivation rate ratio. DF is removed from the upper level by stimulated emission at the rate (gI/ϵ) where I is the radiation intensity in the laser cavity and $\epsilon=h\nu N_A$ is the energy per mole of photons with frequency ν; h is Planck's constant and N_A is Avagadro's number. The ratio of upper state deactivation via stimulated emission to that for collisional deactivation is defined by the parameter $K_2=(2\sigma I)/(\epsilon k_c)$; a radiatively saturated media corresponds to $K_2 \to \infty$. The ratio of the flow to deactivation time is $\zeta=xk_c/u$; ζ_d and ζ_b give the burnout locations for the laminar and strained flames, respectively. In Sec. II, we introduced the strain rate parameter $\lambda=2s_0t_d$; λ defines the strain rate to laminar burn rate ratio. For the laser analysis, it is more appropriate to use a strain rate parameter normalized by the collisional deactivation rate. We therefore define $\gamma=2s_0/k_c$ as the strain to deactivation rate ratio; note γ and λ are related by $\lambda=\zeta_d\gamma$.

Using Eq. (11), the laminar burn time for an oxidizer nozzle of width w is $t_d=0.25(w/B_I)^2/D$. From Fristrom and Westenberg,[12] $D=ET^{5/3}/p$. If D, T, and p have units of cm^2/s, K, and Torr, respectively, then for D_2 diffusing into helium and nitrogen, $E=7.6\times10^{-2}$ and 3.1×10^{-2}, respectively (the values for H_2 fuel are $E=9.3\times10^{-2}$ and 4.2×10^{-2}, respectively). The principal deactivating species in a combustion-driven DF laser are HF and ground state DF, i.e., DF(0). We estimate the mole fraction of DF(0) in the laser cavity as $X_{DF}=0.5X_F$ where X_F is the stream 1 fluorine-atom mole fraction. Using the deactivation rates given by Cohen[13] with DF(2) representing DF_u in the two-level model, then for $T<800$ K, k_c can be approximated by $k_c=3.85\times10^{10}\,(X_{HF}+X_{DF})pT^{-11/5}$ s^{-1}. Since $\zeta_d=k_ct_d$, we can estimate ζ_d for a helium diluent DF laser as

$$\zeta_d=33.4(X_{HF}+X_{DF})\left(\frac{300}{T}\right)^{58/15}(pw)^2 \tag{13}$$

In writing Eq. (13), we have used $B_I=1.00$; this is a representative value for both high- and low-pressure laser conditions. For a nitrogen diluent laser, the values of ζ_d obtained from Eq. (13) should be multiplied by 2.45 to reflect the lower diffusivity. Typical conditions for high-pressure lasers are $X_{HF}=X_F=0.06$, $T=300$ K, $p=12$ Torr, and $w=0.10$-0.20 cm; from Eq. (13) this yields $\zeta_d=4.3$-17.3. For low-pressure lasers, typically, $X_{HF}=X_F=0.15$, $T=300$ K, $p=4$ Torr, and $w=0.15$ cm yielding $\zeta_d=2.7$ (for N_2 diluent, $\zeta_d=6.6$). Thus, for our study, we consider the range $0\le\zeta_d\le20$.

With $\zeta_d \sim (pw)^2$ and $t_d \sim pw^2$, then $\lambda \sim s_0pw$ and $\gamma \sim s_0/p$. We choose to use γ as the characteristic strain rate parameter since it is independent of the nozzle scale w. With ζ_d and γ as the two independent parameters in the model, then for a laser operating at a constant cavity pressure varying γ reflects change in the strain rate while varying ζ_d corresponds to a change in the nozzle scale.

Since $\tau=t/t_d=x/x_d$, then we can use the results from Sec. II to write the flame function in the region $0\le\zeta\le\zeta_b$ and the burnout location in terms of ζ as

$$r(\zeta)=\lambda^{-1/2}[\exp(\gamma\zeta)-1]^{1/2}, \qquad \zeta_b=\gamma^{-1}\ln(1+\lambda) \tag{14}$$

For simplicity of notation, we retain the parameter λ in Eq. (14); λ, however, is not an independent parameter but is calculated from $\lambda=\gamma\zeta_d$.

The starting point for our analysis is the streamline gain equation, i.e. Eq. (9b) of Mirels et al.,[1] which we write as

$$\frac{dg}{d\zeta}+(1+K_2)g=g_0\{(1+K_1)\exp[-K_1(\zeta-\zeta_0)]-1\} \tag{15}$$

Equation (15) defines the influence of pumping, deactivation, and radiative saturation on the gain for a streamline which enters the flame at $\zeta=\zeta_0$. Equation (15) is valid for $\zeta>\zeta_0$ since $g=0$ upstream of the flame. The integrated gain across a channel of width w is

$$G(\zeta)=\int_0^{y^*} g(\zeta,y)\,dy, \qquad \begin{matrix} y^*=y_f^*,\ \zeta\le\zeta_b \\ =w,\ \zeta\ge\zeta_b \end{matrix} \tag{16}$$

We use the effective flame location $y_f^*=wr(\zeta)$ to calculate the gain for the strained flame case. The power extracted from a channel of width w per unit channel height is

$$P(x)=\int_{x_i}^{x}\int_0^{y^*} g(x,y)I(x)\,dy\,dx \tag{17}$$

where x_i defines the start of the power extraction region. The radiation intensity $I(x)$ is assumed constant across the cavity but is allowed to vary in the axial direction.

The chemical energy available for conversion to laser power is $E_c=uw[F]_I\Delta h$ where Δh is the chemical energy released per mole of fluorine-atom reacted by the laser pumping reaction. Define φ as the photon yield per mole of reacted fluorine-atom for a saturated premixed laser and let $(\eta\varphi)$ represent the yield for a diffusion-type laser. The efficiency η represents the power loss due to a finite mixing rate, incomplete saturation, and collisional deactivation. The power in the laser beam is $P=uw[F]_I\epsilon\varphi\eta$ and the chemical conversion efficiency is $\eta_c=P/E_c=(\varphi\epsilon/\Delta h)\eta=\eta_0\eta$ where $\eta_0=\varphi\epsilon/\Delta h$ is the efficiency for the laser operating in the saturated premixed condition. The parameters φ and η_0 are defined by the multivibrational level physics of the lasing process and cannot be calculated from the two-level model. Hofland and Mirels[9] and Mirels[10] give results which indicate η_0 is a function of the temperature in the lasing region and the rotational level (J) of the lasing transition. For $T=300$ K, a representative value φ for both HF and DF lasers is $\eta_0=0.30$ and we will use this as a characteristic value herein. It should be noted that η_0 is not truly independent of the mixing rate since the lasing region temperature T is influenced by mixing,

e.g., faster mixing usually implies a lower value of T due to more efficient diluent utilization and, thus, a higher value for η_0. T and, thus, η_0 are also affected by the laser operating condition, e.g., free jet (constant pressure) or confined cavity (area defined). Since η_0 is affected by many variables, e.g., mixing rate and configuration, accurate estimates for η_c require detailed numerical calculations which can account for all the details of the specific problem under consideration. It is not our purpose to do this herein; rather we use the two-level model to calculate η and show how the faster mixing associated with the strained flow has the potential to improve performance. The strained flow mixing model outlined herein easily can be adapted for use with the more detailed numerical models and this subject will be covered at a later date.

Using Eq. (17), η can be written as

$$\eta=\frac{2P}{\epsilon u w[\mathrm{F}]_1}=\int_{\zeta_i}^{\zeta} G^*(\zeta)K_2(\zeta)\,\mathrm{d}\zeta \tag{18}$$

where $G^*(\zeta)=G(\zeta)/(g_0 w)$. In writing Eq. (18), we have used $\varphi=0.5$ since this value is consistent with the two-level laser model used to define the integrand in Eq. (18). Note that we allow K_2 to be a function of ζ; this differs from the usage of Mirels et al.[1] and we do this so that Eq. (18) can be used to define η for both the amplifier and oscillator configurations.

Amplifier Solution

We assume a beam with a uniform intensity enters the laser cavity and is amplified. The radiation intensity in the cavity is represented by a constant characteristic value I and Eq. (15) is solved using $K_2=\text{const}$. The solution of Eq. (15) given by Mirels et al.[1] can be written as

$$g/g_0=C_1\exp[-K_3(\zeta-\zeta_0)]-C_2\exp[-K_1(\zeta-\zeta_0)]+C_3 \tag{19}$$

where $K_3=(1+K_2)$, $C_1=[D_1(2-D_2)]/(D_1-1)$, $C_2=(1+D_1-D_2)/(D_1-1)$, $C_3=D_2-1$, $D_1=K_1/K_3$, and $D_2=K_2/K_3$. Before using Eq. (16) to calculate $G(\zeta)$ we first change the integration variable from y to ζ_0 using $\mathrm{d}y=(\mathrm{d}r/\mathrm{d}\zeta_0)\mathrm{d}\zeta_0$. Integrating by parts to remove $(\mathrm{d}r/\mathrm{d}\zeta_0)$ yields

$$G(\zeta)=g(\zeta,\zeta^*)r(\zeta^*)-\int_0^{\zeta^*} r(\zeta_0)\left(\frac{\mathrm{d}g}{\mathrm{d}\zeta_0}\right)\mathrm{d}\zeta_0 \qquad \begin{matrix}\zeta^*=\zeta,\zeta\le\zeta_b\\ =\zeta_b,\zeta\ge\zeta_b\end{matrix} \tag{20}$$

Substituting Eq. (19) into Eq. (20) and noting that $g(\zeta,\zeta^*)=0$ for $\zeta\le\zeta_b$ yields

$$G^*(\zeta)=C_2f_2(\zeta)-C_1f_1(\zeta) \qquad \zeta\le\zeta_b \tag{21a}$$

$$=C_1[1-f_1(\zeta_b)]\exp[-K_3(\zeta-\zeta_b)]-C_2[1-f_2(\zeta_b)]\exp[-K_1(\zeta-\zeta_b)]+C_3 \qquad \zeta\ge\zeta_b \tag{21b}$$

The functions $f_1(\zeta)$ and $f_2(\zeta)$, and their series representations (obtained by successive integration by parts) are given by

$$f_i(\zeta)=K_j\exp(-K_j\zeta)\int_0^{\zeta} r(\zeta_0)\exp(K_j\zeta_0)\,\mathrm{d}\zeta_0=\sum_{n=0}^{\infty}(-1)^n\frac{1}{K_j^n}\frac{\mathrm{d}^n r}{\mathrm{d}\zeta_0^n} \tag{22}$$

where for $i=1$ and 2, $K_j=K_3$ and K_1, respectively.

The results in Eqs. (21a) and (21b) represent the most general solutions for the gain for arbitrary values of K_1, K_2, and flame shape. In flame sheet limit, $K_1\to\infty$, $f_2(\zeta)\to r(\zeta)$, and Eqs. (21a) and (21b) reduce to

$$G^*(\zeta)=r(\zeta)-(2-D_2)f_1(\zeta) \qquad \zeta\le\zeta_b \tag{23a}$$

$$=[1-D_2+G^*(\zeta_b)]\exp[-K_3(\zeta-\zeta_b)]+C_3 \qquad \zeta\ge\zeta_b \tag{23b}$$

The gain at the oxidizer burnout point is $G^*(\zeta_b)=1-(2-D_2)f_1(\zeta_b)$. The small-signal gain distributions are obtained from Eqs. (23a) and (23b) by letting $K_2\to 0$, i.e., $K_3\to 1$, $D_2\to 0$, and $C_3\to 1$.

For a saturated media, $K_2\to\infty$, $K_3\to K_2$, $D_2\to 1$, and $C_3\to 0$. To obtain the gain distributions for $K_1\to\infty$ and $K_2\to\infty$, we substitute the series for $f_1(\zeta)$ into Eq. (23a); retaining terms of $0(K_2^{-1})$ yields

$$G^*(\zeta)=\frac{1}{K_2}\left(\frac{\mathrm{d}r}{\mathrm{d}\zeta}-r\right) \qquad \zeta\le\zeta_b \tag{24a}$$

$$=G^*(\zeta_b)\exp[-K_2(\zeta-\zeta_b)] \qquad \zeta\ge\zeta_b \tag{24b}$$

When $K_2\gg 1$, Eq. (24b) indicates $G^*\to 0$ very rapidly in the region $\zeta>\zeta_b$.

Figure 4 shows the small-signal gain ($K_2=0$) distributions calculated using Eqs. (23a) and (23b) and Eq. (14) for $\gamma=0$-8 and for $\zeta_d=1$ and 10. The sharp peak shown in these distributions corresponds to the burnout point $\zeta=\zeta_b$; for $\zeta>\zeta_b$, the gain decays exponentially. For $\zeta_d=1$ it is seen that increasing γ increases the gain, e.g., for $\gamma=3$ the peak gain is 50% higher than the laminar ($\gamma=0$) value while for $\gamma=8$, the peak gain is more than twice the laminar value. When ζ_d is large, the effect of γ on the gain is even more significant, e.g., for $\zeta_d=10$, a value of $\gamma=3$ yields a peak gain more than double the laminar value. The results also show that for all values of γ, when ζ_d is increased the length of the positive gain region also increases. It is noted that increasing γ does not necessarily shorten the gain region, e.g., for $\zeta_d=10$ as γ is increased, the length of the positive gain region first increases, then decreases. Note for $\zeta_d=10$, the positive gain regions for $\gamma=0$ and $\gamma=8$ have about the same length.

Figure 5 shows the gain distributions for a loaded amplifier with $K_2=10$. The saturated gain is significantly lower and shorter than the small-signal gain. While the gain distributions in Fig. 4 are roughly triangular in shape when γ is large, those in Fig. 5 have more complex geometry. This indicates that the small-signal gain distributions (which are often measured) may not provide a good representation for the saturated gain distributions, i.e., the two cannot be related via a simple saturation parameter. This is a significant point in that saturated gain distributions such as shown in Fig. 5 are often used as the media model in complex resonator studies; and, often, these distributions are derived from small-signal gain data. One other feature worth noting in Figs. 4 and 5 is that as $\zeta\to 0$, all the distributions collapse to a single curve. This is due to the fact, noted earlier, that as $\zeta\to 0$, $r(\zeta)$ as given by Eq. (14) reduces to a laminar flame shape.

Oscillator Solution

For a Fabry-Perot laser cavity consisting of two plane parallel mirrors with reflectivities r_1 and r_2 and a nozzle array with N nozzles with half-width w, the normalized threshold gain is $G_t^*=-\ell n(r_1r_2)/(4Ng_0w)$. Lasing starts at ζ_i, defined by $G^*(\zeta_i,K_2=0)=G_t^*$ or $G_I^*(\zeta_i,K_2=0)=\varphi_i$, where $\varphi_i=\zeta_d^{1/2}G_t^*$ and $G_I^*=\zeta_d^{1/2}G^*$ are the parameters used by Mirels et al.[1] to characterize the threshold level.

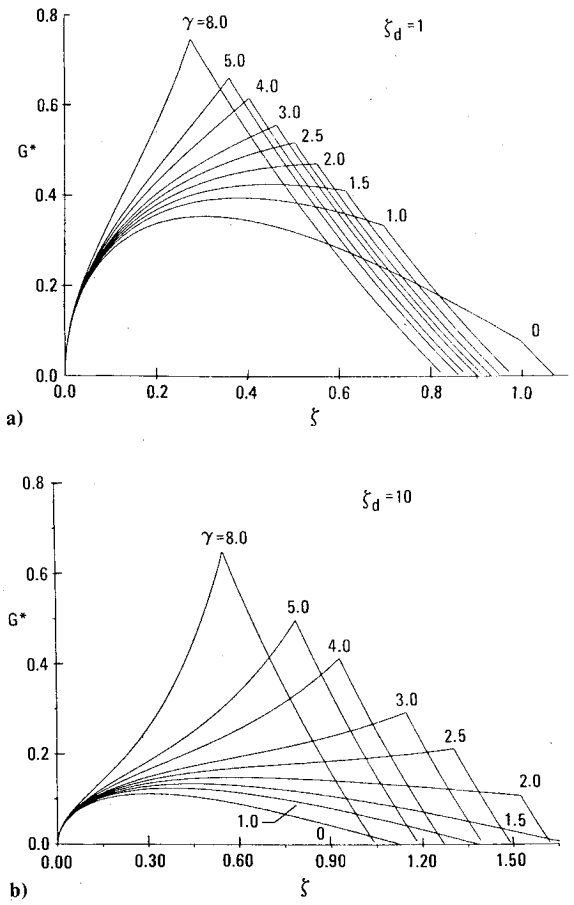

Fig. 4 Small signal gain distributions ($K_2=0$) for $0\le\gamma\le8$, $\zeta_d=1$ and 10.

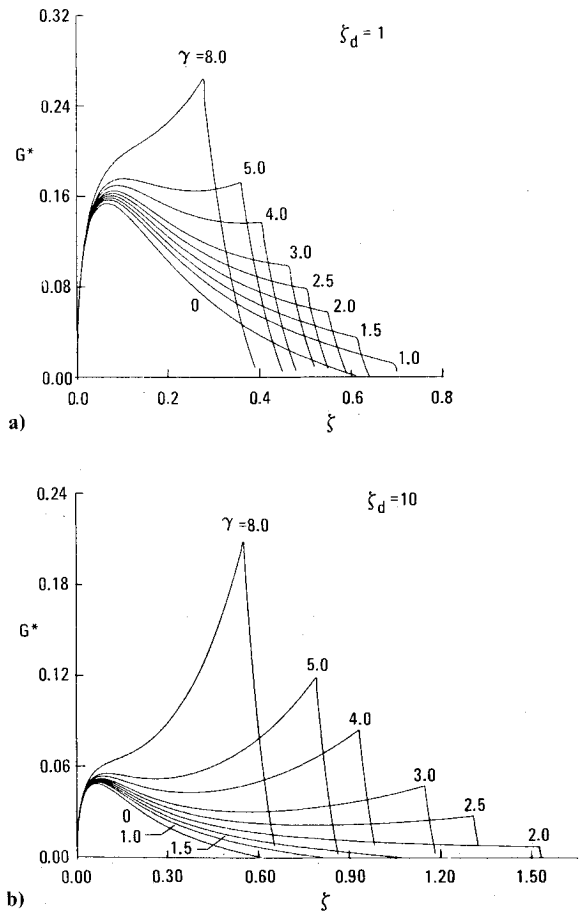

Fig. 5 Gain distributions for $K_2=10$, $0\le\gamma\le8$, $\zeta_d=1$ and 10.

In the lasing region ($\zeta_i\le\zeta\le\zeta_e$), the radiation intensity is found by substituting Eq. (15) to Eq. (16) and solving for $K_2(\zeta)$. In doing this, we use the constant gain approximation, i.e., that $G(\zeta)=G_t$ is the lasing region. The most general result obtained for $K_2(\zeta)$ is

$$K_2(\zeta)=\frac{1}{G_t^*}\left[K_1 r(\zeta)-(1+K_1)f_2(\zeta)\right]-1 \qquad \zeta\le\zeta_b \text{(25a)}$$

$$=K_{2b}-\frac{(1+K_1)}{G_t^*}\left\{1-\exp\left[-K_1(\zeta-\zeta_b)\right]\right\} \qquad \zeta\ge\zeta_b \text{(25b)}$$

where $K_{2b}=K_2(\zeta_b)$.

For $K_1\to\infty$, using Eq. (22) to simplify Eq. (25a) yields

$$K_2(\zeta)=\frac{1}{G_t^*}\left(\frac{dr}{d\zeta}-r\right)-1, \qquad \zeta\le\zeta_b \tag{26}$$

For $\zeta_e\le\zeta_b$, the end of the lasing zone is found from the condition that $K_2(\zeta_e)=0$; from Eq. (26), one obtains

$$\left(\frac{dr}{d\zeta}\right)_{\zeta_e}-r(\zeta_e)=G_t^* \tag{27}$$

As $K_1\to\infty$, Eq. (25b) implies that for $\zeta_e>\zeta_b$, then $(\zeta_e-\zeta_b)=0(K_1^{-2})$; thus, when $\zeta_e>\zeta_b$ and $K_1\gg1$, $\zeta_e\approx\zeta_b$. The laser efficiency is obtained by substituting Eq. (26) into Eq. (18) yielding

$$\eta=r(\zeta_e)-r(\zeta_i)-\int_{\zeta_i}^{\zeta_e} r(\zeta)\,d\zeta-G_t^*(\zeta_e-\zeta_i) \tag{28}$$

For $G_t\to0$, then $\zeta_i\to0$ and Eq. (28) reduces to

$$\eta=r(\zeta_e)-\int_0^{\zeta_e} r(\zeta)\,d\zeta \tag{29}$$

It easily is shown using Eqs. (18) and (24) that this same result is obtained for the power extraction efficiency of a saturated ($K_2\to\infty$) amplifier. Mirels et al.[1] use a flame function with the form $r(\zeta)=(\zeta/\zeta_b)^n$ to calculate η for laminar ($n=0.5$) and turbulent ($n=1.0$) mixing. If this function is substituted into Eq. (24), the results given by Mirels et al.[1] will be recovered.

From Eq. (14), one has $(dr/d\zeta)=(1+\lambda r^2)/(2\zeta_d r)$. Using the result in Eq. (27) and solving for $r_e=r(\zeta_e)$ yields

$$r_e=\frac{1}{\zeta_d^{1/2}(2-\gamma)^{1/2}}\left\{\left[1-\frac{\varphi_1^2}{(2-\gamma)}\right]^{1/2}-\frac{\varphi_i}{(2-\gamma)^{1/2}}\right\} \tag{30}$$

To obtain ζ_e, we invert Eq. (14) to obtain $\zeta_e=\gamma^{-1}\ell n(1+\lambda r_e^2)$. Equation (30) is valid for $\zeta_e\le\zeta_b$, $r_e\le1$. No real solutions are obtained for $\gamma\ge2$. Define ζ_{dj} by the condition that $r_e(\zeta_{dj})=1$; from Eq. (30) it can be shown that $\zeta_{dj}=[2(1+G_t^*)-\gamma]^{-1}$. The significance of ζ_{dj} is that for given values of $\gamma<2(1+G_t^*)$ and G_t^*, it defines the value of ζ_d separating the complete and incomplete burning modes. If $\zeta_d>\zeta_{dj}$, then $\zeta_e<\zeta_b$ and lasing stops before the oxidizer is fully reacted; when $\zeta_d<\zeta_{dj}$, then $\zeta_e\approx\zeta_b$ and all the fluorine is burned in the lasing region. For a saturated oscillator ($G_t\to0$), these results imply that when $\gamma\ge2$, the fluorine is always fully utilized; incomplete burning corresponds to the narrow region of $0\le\gamma<2$.

Substituting Eq. (14) into Eq. (28) and evaluating the integral yields

$$\eta=\left\{r-\frac{2}{\gamma}\left[r-\frac{1}{\lambda^{1/2}}\tan^{-1}(\lambda^{1/2}r)\right]-G_t^*\zeta\right\}_{\zeta_i r_i}^{\zeta_e r_e} \tag{31}$$

where for $\zeta_e<\zeta_b$, r_e is obtained for Eq. (30) while for $\zeta_e>\zeta_b$, then $r_e=1$. For a saturated oscillator, G_t^* and $\zeta_i\to 0$, and Eq. (30) reduces to $r_e=[\zeta_d(2-\gamma)]^{-1/2}$. Thus, Eq. (31) reduces to

$$\eta=1-\frac{2}{\gamma}\left[1-\frac{1}{\lambda^{1/2}}\tan^{-1}(\lambda^{1/2})\right] \qquad \zeta_d\le\zeta_{dj},\ \zeta_e\approx\zeta_b \tag{32a}$$

$$=\frac{1}{\lambda^{1/2}}\left[\frac{2}{\gamma}\tan^{-1}\left(\frac{\gamma}{\gamma-2}\right)^{1/2}-\left(\frac{\gamma-2}{\gamma}\right)^{1/2}\right]$$

$$\zeta_d\ge\zeta_{dj},\ \zeta_e\le\zeta_b \tag{32b}$$

As $\gamma\to 0$ and $\lambda\to 0$, it easily is shown that Eqs. (32a) and (32b) produce the laminar results of Mirels et al.[1]

Figure 6 shows the laser efficiency η for a saturated oscillator as a function of γ and ζ_d. As $\zeta_d\to 0$, all curves approach the premixed result of $\eta=1$. For low values of γ, η drops very rapidly as ζ_d increases. When $\gamma<2$ and $\zeta_d>\zeta_{dj}$, lasing stops before the fluorine is completely burned; in this region, Eq. (32b) indicates that for any value of γ, $\eta\sim\zeta_d^{-1/2}\sim(pw)^{-1}$. For $\gamma>2$, all the fluorine is burned in the lasing region and Eq. (32a) implies that as $\zeta_d\to\infty$, $\eta\to(1-2/\gamma)$, i.e., there is an asymptotic value below which the efficiency does not fall.

A measure of the laser power output is $P^*=\zeta_d^{1/2}\eta$. P^* represents the power per channel for fixed values of stoichiometry, temperature, and flow velocity; thus, varying ζ_d corresponds to changing p or w. Figure 7 shows the results for P^*. For $\gamma<2$ and $\zeta_d>\zeta_{dj}$, P^* is invariant with ζ_d and a function of γ only. This result was reported previously by Mirels et al.[1] and Broadwell[2] for the laminar and turbulent mixing cases, respectively. It implies that as the cavity pressure or laser mass flow is increased, the laser power remains constant. This result is not in agreement with the operating characteristics of trip nozzle lasers where it is found that the laser power increases as the mass throughput is increased. The strained flame model indicates that for $\gamma>2$, P^* continues to increase as ζ_d increases, i.e., power continues to increase with mass throughput. Equation (32a) implies that when $\lambda=\gamma\zeta_d$ is large, then η approaches a constant value and $P^*\sim\zeta_d^{1/2}\sim(pw)$, i.e, the power increases linearly with cavity pressure or mass flow.

Figure 8 shows η and P^* normalized by the laminar mixing ($\gamma=0$) results for the range of $\zeta_d\le 5$. Even modest values of γ yield large increases in power, e.g., for $\zeta_d=5$, a factor of two increase in power is achieved at the $\gamma=2.5$ level. It is significant that even at low values of ζ_d performance can be improved by straining the flow, e.g., for $\zeta_d=2$, the laser power is doubled when compared to the laminar results when $\gamma=5$.

Figure 9 shows the lasing zone length ζ_e. For $\gamma<2$ and $\zeta_d>\zeta_{dj}$, ζ_e is independent of ζ_d and a function of γ only. For $\gamma<2$, it is seen that ζ_e increases as γ increases. For $\gamma>2$, the

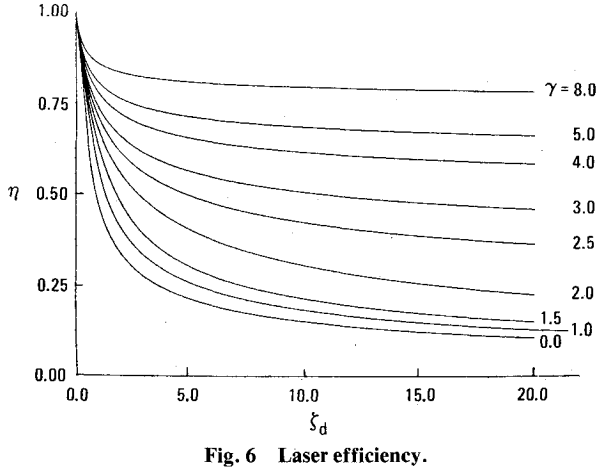

Fig. 6 Laser efficiency.

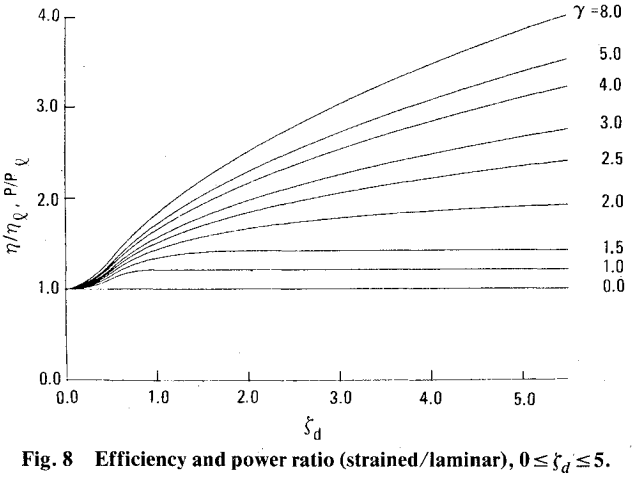

Fig. 8 Efficiency and power ratio (strained/laminar), $0\le\zeta_d\le 5$.

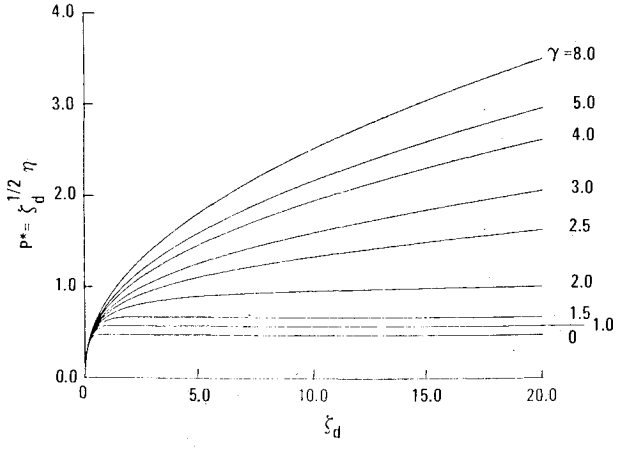

Fig. 7 Laser power.

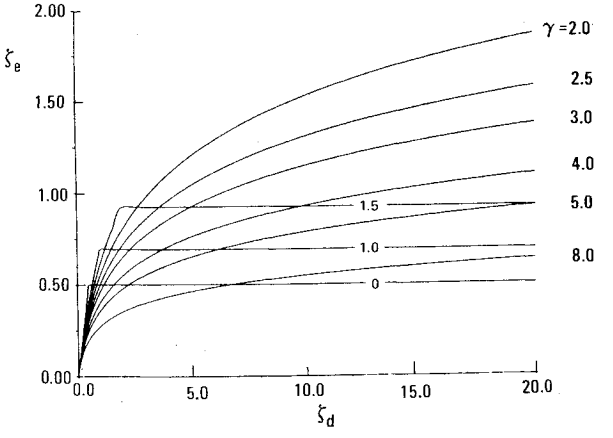

Fig. 9 Lasing zone length.

trend reverses and ζ_e decreases as γ is increased. This result is expected from Eq. (14) since $\zeta_e = \zeta_b$ for $\gamma > 2$. The trend that ζ_e increases with ζ_d is also expected from Eq. (14). For $\gamma > 2$, the lasing zone lengths for the most part are longer than the laminar mixing values. Thus, the results indicate that a large value of γ does not imply a short lasing zone.

IV. Discussion

Trip Nozzle Lasers

This is not the place for an exhaustive analysis of trip nozzle data, however, it is appropriate to show that the strained flow laser model is in qualitative agreement with trip nozzle data trends. Quantitative agreement is not to be expected due to the many simplifications inherent in the analytical model; this issue is best left for detailed numerical studies.

Wilson and Hook[4] report trip nozzle laser efficiencies in the $\eta_c = 0.10$-0.15 range and that trip jet injection increases laser power by about 80% when compared to the laminar mixing case. The results from more recent trip nozzle experiments showed power increases in the 2.0-2.5 range. Helium diluent DF lasers with trip nozzles generally have characteristic values of ζ_d in the 4-6 range. For lasers with $\zeta_d \approx 5$ operating at twice the laminar power level, Fig. 8 implies an effective value of γ in the 2-3 range. For $\zeta_d = 5$ and $\gamma = 2.5$, then from Fig. 6, $\eta = 0.49$; with $\eta_0 = 0.30$ then $\eta_c = 0.15$ which is consistent with trip nozzle data. A characteristic of the strained flow model shown in Fig. 6 is the slow decrease in η as ζ_d increases. This result also explains a trend observed in trip nozzle data, i.e., that performance is relatively insensitive to nozzle size. The laminar and turbulent models of Mirels et al.[1] and Broadwell[2] cannot explain this phenomenon, e.g., when $\zeta_d > 1$, they predict $\eta \sim (pw)^{-1}$ which indicates a sensitivity to cavity pressure and nozzle scale not observed in trip nozzle data. These earlier models also predict that for $\zeta_d > 1$, laser power is constant while our model indicates that when $\gamma > 2$, power increases with ζ_d; it is the latter trend which is observed in tripped flow data. Our conclusion from this comparison is that the laminar and turbulent models of Mirels et al.[1] and Broadwell[2] are not in agreement with the characteristics shown by the trip nozzle data while the strained flow laser model does show the proper behavior and indicates that $\gamma = 2$-3 is an appropriate characteristic value for nozzles using gas jet trips within the context of the constant strain rate distribution function used herein. This strain rate distribution was used to illustrate the character of the model and is not intended to imply that trip nozzles generate constant strain rates. Clearly, more information is needed on the actual strain rate distribution associated with trip nozzles in order to apply the reactant-surface stretching approach outlined herein in a more quantitative manner.

Trip nozzles use helium jets with a mass flowrate of about 5% of the total laser flow. Increasing the trip flowrate above this level usually results in a constant or reduced laser power. This appears to imply that above a certain level, increasing the trip flow does not appreciably increase the strain parameter γ; the situation, however, is actually more complex than this. One would expect the strain rate parameter γ to scale with the trip jet penetration h_j. Zukoski and Spaid[8] indicate $h_j \sim m_j^{1/2}$ where m_j is the jet mass flowrate. If $\gamma \sim h_j \sim m_j^{1/2}$, then the strain should increase continually with the jet mass flow. Since the trip jets are located between the fuel and oxidizer streams, they create a helium layer between the two reactant streams in at least part of the flow. The fuel and oxidizer must diffuse across this layer before they can react. While increasing the trip flow should increase γ, it also increases the width of the helium layer across which the reactants must diffuse. This suggests that above the 5% trip flow level, any increase in the mixing due to an increase in trip flow is balanced by a reduction in the mixing rate associated with the increased helium barrier layer size. The net effect is that laser power does not increase for trip flows above the 5% level and that gas trip lasers are effectively limited to operating in the $\gamma = 2$-3 regime. The results in Fig. 8 indicate that if nozzles can be designed to operate at $\gamma > 3$, significant increases in laser power above that available from current designs can be expected. Since the $\gamma > 3$ region is apparently not accessible via gas trip nozzle designs, new nozzle designs which induce strain into the flow using another mechanism are required.

Low-Pressure Nozzle Designs

Lasers designed for use at low cavity pressures (3-7 Torr) do not currently use trip jets or other mixing enhancement devices; they rely on molecular diffusion to mix the reactants. Figure 8 illustrates the potential for strain-accelerated mixing to improve performance at low values of ζ_d. For $\zeta_d = 2.5$, which represents low-pressure helium diluent lasers, operating at $\gamma = 2.0$ yields a 72% power increase over the laminar results which at $\gamma \approx 3$, the laser power about doubles. For $\zeta_d = 6.0$, which characterizes low-pressure nitrogen diluent lasers, the performance improvement potential is even larger due to lower molecular diffusivities associated with the nitrogen. For example, with $\zeta_d = 6.0$ and $\gamma = 2.0$, power increases by 93% while for $\gamma = 3$, an 180% increase is obtained. These results suggest that there is much that can yet be done to improve the mixing, and, thus, efficiency, for low-pressure laser designs and that it could be advantageous to explore nozzle designs which will introduce strain into such flows.

V. Summary and Conclusions

In this paper we have introduced the idea that gas jet trip nozzles improve laser performance over laminar mixing designs by generating a secondary flow at the nozzle exit plane which stretches the reactant surfaces, thereby increasing the contact area between the reactant streams, and, thus, the reactant mixing rates. This process is described by ascribing an induced strain rate to the trip jets and then by developing a flow model for burning in the presence of a strain field. The flow model was coupled to a laser performance model in order to define the influence of the strain rate on the laser efficiency. Strain enters the model via a single parameter $\gamma = 2s_0/k_c$ which is the ratio of the strain rate to deactivation rate. In the fast pumping limit, the model indicates that for a saturated oscillator $\gamma = 2$ is a junction point for the burning modes with the fluorine always being fully burned in the lasing zone when $\gamma > 2$. The strained flow model is shown to be in better agreement with trip flow laser data than previous laminar and turbulent mixing laser models with the data implying effective values of γ in the 2-3 range for gas jet trip nozzles. The results from the model suggest that the performance of high-pressure lasers could be improved if a passive (no gas injection) strain-generating mechanism yielding $\gamma > 3$ were used. The model results also indicate that the performance of low-pressure nozzles, which currently operate in the laminar mixing mode, could be significantly improved by implementing the strain-accelerated mixing concept discussed herein. In fact, if a passive mechanism for generating high strain levels ($\gamma = 5$-8) could be developed, the model results would imply that it should be possible to double the laser performance over current designs for both low- and high-pressure laser designs.

Acknowledgment

This work was supported under the 1981 Bell Aerospace IR&D program.

References

[1] Mirels, H., Hofland, R., and King, W. S., "Simplified Model of CW Diffusion-Type Chemical Laser," *AIAA Journal*, Vol. 11, Feb. 1973, pp. 156-164.

[2] Broadwell, J. E., "Effect of Mixing Rate on HF Chemical Laser Performance," *Applied Optics*, Vol. 13, April 1974, pp. 962-967.

[3]Witte, A. B. et al., "Aerodynamic Reactive Flow Studies of the H_2/F_2 Laser-II," AFWL-TR-74-78, Aug. 1974.

[4]Wilson, L. E. and Hook, D. L., "Deuterium Fluoride CW Chemical Laser," AIAA Paper 76-344, San Diego, Calif., 1976.

[5]Driscoll, R. J. and Tregay, G. W., "Flowfield Experiments on a Tripped DF Chemical Laser," AIAA Paper 81-1271, Palo Alto, Calif., 1981.

[6]Cenkner, A. A., "Laser Doppler Velocimeter Measurements on Supersonic Mixing Nozzles that Employ Gas Trips," *AIAA Journal*, Vol. 20, March 1982, pp. 383-389.

[7]O'Keefe, D., Sugimura, T., Behrens, W., Bullock, D., and Dee, D., "Comparison of LAMP and BLAZER Code Calculations with CL-XV Measurements," *Optical Engineering*, Vol. 18, July-Aug. 1979, pp. 363-369.

[8]Zukoski, E. E. and Spaid, F. W., "Secondary Injection to Gases into a Supersonic Flow," *AIAA Journal*, Vol. 2, Oct. 1964, pp. 1689-1696.

[9]Hofland, R and Mirels, H., "Flame-Sheet Analysis of CW Diffusion-Type Chemical Lasers, I. Uncoupled Radiation," *AIAA Journal*, Vol. 10, April 1972, pp. 420-428.

[10]Mirels, H., "Simplified Model of a Continuous Wave Diffusion-Type Chemical Laser—An Extension," *AIAA Journal*, Vol. 14, July 1976, pp. 930-939.

[11]Gross, R. W. F. and Bott, J. F., eds., *Handbook of Chemical Lasers*, Wiley, New York, 1976, pp. 344-382.

[12]Fristrom, R. M. and Westenberg, A. A., *Flame Structure*, McGraw Hill, New York, 1965, p. 276.

[13]Cohen, N., "A Review of Rate Coefficients in the D_2-F_2 Chemical Laser System," The Aerospace Corp., Los Angeles, Calif., SAMSO-TR-77-152, Aug. 1977.